Osterberg, F., Cerne, J., Shyamsunder, E., Gruner, S. M., Lamparski, H., & O'Brien, D. F. (1991) *Biophys. J. 59*, 128a.
Parsegian, V. A., Fuller, N., & Rand, R. P. (1979) *Proc. Natl. Acad. Sci. U.S.A. 76*, 2750-2754.
Pidgeon, C., & Hunt, C. A. (1983) *Photochem. Photobiol. 37*, 491-494.
Pidgeon, C., & Hunt, C. A. (1987) *Methods Enzymol. 149*, 99-111.
Rand, R. P. (1981) *Annu. Rev. Biophys. Bioeng. 10*, 277-314.
Regen, S. L. (1987) in *Liposomes: From Biophysics to Therapeutics* (Ostro, M. J., Ed.) p 73, Marcel Dekker, New York.
Ringsdorf, H., & Laschewsky, A. (1988) *Marcromolecules 21*, 1936-1941.
Ringsdorf, H., Schlarb, B., & Venzmer, J. (1988) *Angew. Chem., Int. Ed. Engl. 27*, 113-158.
Seddon, J. M. (1990) *Biochim. Biophys. Acta 1031*, 1-69.
Shyamsunder, E., Gruner, S. M., Tate, M. W., Turner, D. C., So, P. T. C., & Tilcock, C. P. S. (1988) *Biochemistry 27*, 2332-2336.
Siegel, D. P. (1984) *Biophys. J. 45*, 399-420.
Siegel, D. P. (1986a) *Biophys. J. 49*, 1155-1170.
Siegel, D. P. (1986b) *Biophys. J. 49*, 1171-1183.
Siegel, D. P. (1987) *Chem. Phys. Lipids 42*, 279-301.
Siegel, D. P., Burns, J. L., Chestnut, M. H., & Talmon, Y. (1989a) *Biophys. J. 56*, 161-169.
Siegel, D. P., Banschbach, J., Alford, D., Ellens, H., Lis, L. J., Quinn, P. J., Yeagle, P. L., & Bentz, J. (1989b) *Biochemistry 28*, 3703-3709.
Strolley, J. G., & Vail, W. J. (1977) *Biochim. Biophys. Acta 471*, 372-390.
Szoka, F. C., & Papahadjopoulos, D. (1978) *Proc. Natl. Acad. Sci. U.S.A. 75*, 4194-4198.
Talmon, Y., Burns, J. L., Chestnut, M. H., & Siegel, D. P. (1990) *J. Electron Microsc. Tech. 14*, 6-12.
Tilcock, C. P. S., Bally, M. B., Farren, S. B., & Cullis P. R. (1982) *Biochemistry 21*, 4596-4601.
Tyminski, P. N., Latimer, L. H., & O'Brien, D. F. (1985) *J. Am. Chem. Soc. 107*, 7769-7770.
Tyminski, P. N., Ponticello, I. S., & O'Brien, D. F. (1987) *J. Am. Chem. Soc. 109*, 6541-6542.
Tyminski, P. N., Latimer, L. H., & O'Brien, D. F. (1988) *Biochemistry 27*, 2696-2705.
Van Dijck, P. W. M., de Kruijff, B., Van Deenen, L. L. M., de Grier, J., & Demel, R. A. (1976) *Biochim. Biophys. Acta 455*, 576-587.
Veiro, J. A., Khalifah, R. G., & Rowe, E. (1990) *Biophys. J. 57*, 637-641.
Verkleij, A. J. (1984) *Biochim. Biophys. Acta 779*, 43-66.
Verkleij, A. J., de Maagd, R., Leunissen-Bijvelt, J., & de Kruijff, B. (1982) *Biochim. Biophys. Acta 684*, 255-262.
You, H., & Tirrell, D. A. (1991) *J. Am. Chem. Soc. 113*, 4022-4023.

Investigation of Heme Distortions and Heme–Protein Coupling in the Isolated Subunits of Oxygenated Human Hemoglobin by Resonance Raman Dispersion Spectroscopy

Reinhard Schweitzer-Stenner,* Uwe Dannemann, and Wolfgang Dreybrodt
Institute of Experimental Physics, University of Bremen, 2800 Bremen 33, Germany
Received June 27, 1991; Revised Manuscript Received October 10, 1991

ABSTRACT: To probe the distortions of the heme groups resulting from heme–apoprotein interaction in the isolated subunits of oxygenated human hemoglobin (i.e., α^{SH}-oxyHbA and β^{SH}-oxyHbA), the dispersion of the depolarization ratio of the Raman lines at 1375 cm^{-1} (ν_4) and 1638 cm^{-1} (ν_{10}) was measured at various pHs. The data were analyzed in terms of vibronic coupling parameters which depend on symmetry-classified normal distortions of the heme groups. In the α-chain the ν_{10} mode is not affected by symmetry-lowering distortions. In the β-chain, however, this mode is significantly influenced by asymmetric B_{1g} and B_{2g} distortions. This was interpreted in terms of different interactions between the peripheral substituents and the porphyrin macrocycle in the respective chains. The ν_4 mode of both chains is subject to B_{1g} (B_{2g}) and A_{2g} distortions, which are more pronounced in β^{SH}-oxyHbA. This is most probably due to differences in the repulsive interactions between the proximal imidazole and the pyrrole. While the depolarization ratio of both lines investigated is pH-independent in α^{SH}-oxyHbA, it exhibits a significant pH dependence in β^{SH}-oxyHbA. This parallels the finding that the isolated β-chains exhibit a Bohr effect whereas the α-chains do not. Consequently, the pH dependence of the coupling parameters and the Bohr effect of β^{SH}-oxyHbA could be rationalized in terms of the very same proton binding processes. Moreover, the Raman data correlate with low-temperature kinetic measurements by DeIorio et al. [(1990) *Biophys. J. 59*, 1-13] which reveal that the β^{SH}-Hb exhibits a larger structural heterogenity than α^{SH}-Hb. This indicates that the normal distortions monitored by vibronic coupling matrix elements are provided by different conformational substates of the porphyrin macrocycle.

The thorough understanding of cooperativity of oxygen binding to hemoglobin requires knowledge about the modulation of the tertiary structure of its subunits by their aggregation into functional $\alpha_2\beta_2$ tetramers. Moreover, it is im-

0006-2960/92/0431-694$03.00/0

portant to gain information about functional and structural differences between the α- and β-subunits. This can be achieved by investigating the individual subunits which can be isolated in a functional form, thus allowing the reconstitution of intact HbA[1] from mixtures of isolated α- and β-chains (α^{SH}-HbA and β^{SH}-HbA) (Bucci et al., 1965; Winterhalter & Colosimo, 1971). While oxygen binding to α^{SH}-HbA is noncooperative and pH-independent, the binding isotherms of the β-subunits exhibit a Hill coefficient of 1.3 (Benesch et al., 1961) and a small but significant Bohr effect (McDonald & Noble, 1972; Kurtz & Bauer, 1978). In addition, proton binding and ligand binding affect the tetramer–monomer equilibrium of β^{SH}-HbA (McDonald et al., 1987). More recently, flash photolysis experiments were carried out on isolated subunits to study the effect of protein dynamics on their functional properties. By analyzing CO rebinding at various temperatures between 10 and 300 K, Wintherhalter and Di Iorio (1987) and DiIorio et al. (1991) found the distribution of the activation enthalpy for CO rebinding to be much narrower in α^{SH}-HbA than in β^{SH}-Hb. This indicates significant differences in the flexibility of the corresponding structures. Furthermore, DiIorio et al. (1991) found that only the activation enthalpy distribution (DAE) of β^{SH}-HbA depends on the viscosity of the solvent. Together with the observed differences in the Bohr effect this suggests that heme–protein coupling in β^{SH}-HbA is different from that in α^{SH}-HbA.

In the present study Raman dispersion spectroscopy is applied to probe the asymmetric perturbations affecting the prosthetic group in α^{SH}-oxyHbA and β^{SH}-oxyHbA, respectively. This was done by measuring and analyzing the depolarization ratio dispersion (DPD) of Raman lines of the porphyrin macrocycle which are sensitive to structural changes induced by heme–protein interactions.

This procedure provides vibronic coupling parameters which can be assigned to symmetry-classified normal distortions of the functional heme group (Schweitzer-Stenner, 1989). They serve as a suitable tool to monitor even subtle changes of heme–protein coupling as caused by protonation processes in the protein.

Theoretical Background

Raman Scattering on Distorted Porphyrins. To gain information on the molecular basis of heme–protein coupling in the isolated subunits, we apply Raman dispersion spectroscopy to α^{SH}-oxyHbA and β^{SH}-oxyHbA. It is based on the following principles: In its ideal configuration the symmetry of the porphyrin macrocycle is D_{4h}. In this case the depolarization ratio ρ (DPR) of the Raman lines is 0.125 for symmetric A_{1g} modes, 0.75 for asymmetric B_{1g} and B_{2g} modes, and infinite for antisymmetric A_{2g} modes independent of the wavelength of the exciting radiation (Spiro & Strekas, 1974). The corresponding polarizability tensor can be formulated in terms of McClain tensors $\mathbf{T}^{\Gamma}$ ($\Gamma = A_{1g}$, B_{1g}, B_{2g}, and A_{2g}) as follows (McClain, 1970):

$$\alpha^{\Gamma} = a^{\Gamma}(\Omega_L)\mathbf{T}^{\Gamma} \qquad (1)$$

where

$$\mathbf{T}^{A_{1g}} = \begin{bmatrix} 1 & 0 \\ 0 & 1 \end{bmatrix} \mathbf{T}^{B_{1g}} = \begin{bmatrix} 1 & 0 \\ 0 & -1 \end{bmatrix} \mathbf{T}^{B_{2g}} = \begin{bmatrix} 0 & 1 \\ 1 & 0 \end{bmatrix} \mathbf{T}^{A_{2g}} = \begin{bmatrix} 0 & 1 \\ -1 & 0 \end{bmatrix}$$

The constants $a^{\Gamma}(\Omega_L)$ are determined by the transition moments of the electronic dipole transition involved (i.e., between the ground state $|g\rangle$ and the excited electronic state $|e\rangle = |Q_x\rangle$, $|Q_y\rangle$, $|B_x\rangle$, and $|B_y\rangle$), the specific vibronic coupling matrix elements of the considered Raman-active mode, and the frequency (Ω_L) of the incident laser light. Resonance Raman scattering is obtained if Ω_L is close to the resonance conditions $\Omega_L = E_e - E_g$ or $\Omega_L = E_e + \Omega_R = \Omega_L$, where Ω_R is the frequency of the Raman mode and E_e and E_g are the energies of the excited and ground state, respectively. Since z-polarized transitions are not considered, all McClain tensors can be written as 2×2 tensors (Schweitzer-Stenner, 1989). This consideration remains also valid for the symmetries D_4, C_{4h}, and D_{2d}, which do not exhibit an inversion center. Therefore, the out-of plane modes with the odd representations A_{1u}, A_{2u}, B_{1u}, and B_{2u}, which are not Raman active in D_{4h}, collapse into one common representation with the corresponding even symmetries in D_{4h}, C_{4h}, and D_{2d}, thus yielding A_1, A_2, B_1, and B_2, and become Raman active. Their polarizability can be expressed in terms of the very same McClain tensors as the corresponding D_{4h} modes.

Any asymmetric distortions reducing the symmetry of the heme further introduce new components into the Raman tensors of the even heme modes. In this case the polarizability tensor must be written as a linear combination of McClain tensors (Collins et al., 1973; Zgierski & Pawlikowski, 1982; Schweitzer et al., 1982):

$$\alpha^{\Gamma} = \sum_{\Gamma} a^{\Gamma}(\Omega_L)\mathbf{T}^{\Gamma} \qquad (2)$$

Since the frequency dependence of $a^{\Gamma}(\Omega_L)$ is different for the distinct Γ of the Raman-active modes, interference effects between different a^{Γ} occur. Thus the depolarization ratio becomes dependent on the frequency of the exciting light (depolarization ratio dispersion (DPD). Consequently the existence of DPD suggests that the porphyrin macrocycle is subject to asymmetric perturbations.

These induce distortions which result from electronic interactions between the peripheral substituents (PS) of the C_β-carbons and the macrocycle (Shelnutt & Oritz, 1985) and from heme–protein coupling via (a) the coordinative Fe^{2+}–N_ϵ[His(F8)] bond (Šrajer et al., 1986, 1988), (b) repulsive interactions between the proximal imidazole and the nitrogen atoms of the pyrroles (Gellin & Karplus, 1977; Warshel, 1977, Baldwin & Chotia, 1979; Friedman, 1985), and (c) noncovalent bonding between the PS and specific amino acid residues of the heme cavity (Gellin & Karplus, 1977; Shaanan, 1983).

We describe these general distortions in terms of normal distortions $\delta Q_j^{\Gamma(j)}$ of the porphyrin which are classified in terms of the same representations $\Gamma(j)$ as the Raman-active modes [cf. Schweitzer-Stenner (1989)]. They can be regarded either as static or as slow motions of the porphyrin ring with the same pattern as the normal modes, which proceed, however, many orders of magnitude slower than the vibrations of the Raman-active modes (Frauenfelder et al., 1979; Parak et al., 1981; Šrajer et al., 1986; Šrajer & Champion, 1991).

In order to compute the polarizability tensor of a distorted molecule, the vibronic interaction operator is expanded in first order to δQ^{Γ} with respect to the D_{4h} symmetry of the heme

[1] Abbreviations: HbA, human hemoglobin; oxy-HbA, oxygenated human hemoglobin; α^{SH}-oxyHbA and β^{SH}-oxyHbA, ligated isolated α- and β-subunits from HbA with free SH groups; DPR, depolarization ratio; DPD, depolarization ratio dispersion; REP, resonance excitation profile; PS, peripheral substituents of the heme group; DAE, distribution of activation enthalpies; RTC, Raman titration curves; TDR, time-dependent perturbation theory of the Raman scattering.

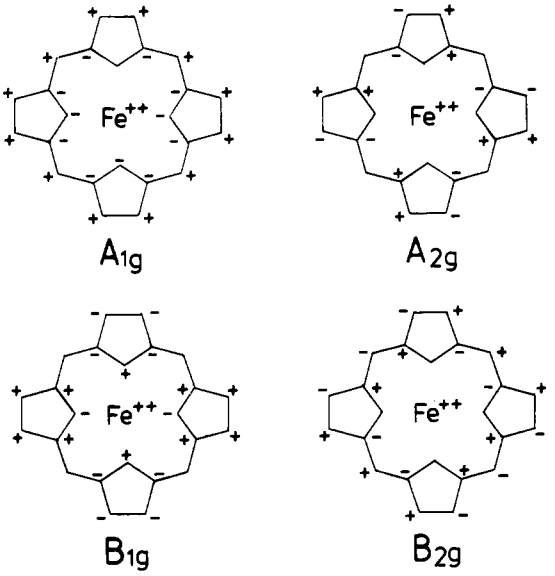

FIGURE 1: Schematic representation of the symmetries of mixing the components of the Q- and B-states of a porphyrin molecule [taken from Shelnutt (1980)].

ring. This yields the following vibronic coupling matrix elements:

$$c^{\Gamma}_{es} = \langle e|dH_{el}/dQ_R^{\Gamma(R)}\delta_{\Gamma(R)\Gamma(j)}|s\rangle + \langle e|\sum_{\Gamma(j)}[d^2H_{el}/dQ_R^{\Gamma(R)}dQ_j^{\Gamma(j)}]\delta Q_j^{\Gamma(j)}|s\rangle Q_R^{01} \quad (3)$$

where $|e\rangle$, $|s\rangle = |Q_x\rangle$, $|Q_y\rangle$, $|B_x\rangle$, and $|B_y\rangle$ are the excited states of the porphyrin molecule expressed in terms of Gouterman's four-orbital model (Gouterman, 1959), H_{el} is the electronic Hamiltonian, and $dH_{el}/dQ_R^{\Gamma(R)}$ is the vibronic coupling operator of the Raman mode exhibiting the symmetry $\Gamma(R)$ in ideal D_{4h}, and $dH^2_{el}/dQ_R^{\Gamma(R)}\delta Q_j^{\Gamma(j)}$ is related to changes resulting from the symmetry-classified perturbations $\delta Q_j^{\Gamma(j)}$. Q_R^{01} is the transition matrix element of the Raman vibration. $\delta_{\Gamma(R)\Gamma(j)}$ is the Kronecker symbol. The sum $\sum_{\Gamma(j)}$ runs over all irreducible representations of the Raman-active modes, thus giving rise to the mixing of different symmetries described by eq 3.

An alternative representation of symmetry-lowering distortions has been given by other authors (Shelnutt, 1980; Zgierski & Pawlikowski, 1982). They expressed them in terms of an electronic perturbation potential $V(q,Q)$ (q: electronic coordinates; Q: nuclear coordinates). It can be decomposed into contributions $V_j^{\Gamma(j)}$ of different symmetry $\Gamma(j)$ (i.e., the symmetries of the Raman-active modes). The corresponding vibronic coupling operator is written as $dV_j^{\Gamma(j)}/dQ_R^{\Gamma(R)}$ and transforms like the product representation $\Gamma(j) \times \Gamma(R)$. Thus it is equivalent to the second derivative in eq 3.

To evaluate in detail the influence of heme–protein interaction on the symmetry properties of the porphyrin, we utilize the schematic representations of Goutermann (1959) as a tool to decompose arbitrary distortions of the molecule into their symmetry-classified contributions (Figure 1). If there is a perturbation at a given atom of the macrocycle, one can find from the sign at that site in the different diagrams whether a respective contribution of symmetry Γ (as given in the diagram) is existing. If two or more equivalent perturbations exist at different sites, the amount of the symmetry-classified contributions of the respective representation is given by adding up all plus and substracting all minus signs.

Reversing this procedure, one can find via which atoms perturbations of symmetry Γ contribute to the matrix element

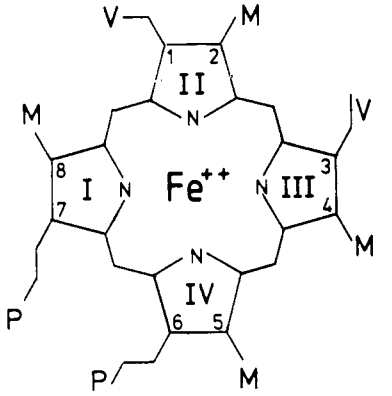

FIGURE 2: Structure of iron(II) protoporphyrin IX. The peripheral substituents are abbreviated by V (vinyl), M (methyl), and P (propionic acid).

c^{Γ}_{es}. If such perturbations of type Γ exist, we can deduce the symmetry of the second derivative in eq 3 by the rule $\Gamma = \Gamma(R) \times \Gamma(j)$ (Shelnutt, 1980). It is important to note that atoms showing a zero in the corresponding diagram do not contribute. These atoms are C_m for $\Gamma = B_{1g}$, A_{2g}, and N_p for $\Gamma = B_{2g}$, A_{2g}.

Figure 1 also shows how the D_{4h} symmetry is lowered by a distinct symmetry-classified distortion. Obviously, A_{1g} distortions do not cause any symmetry lowering, because they cause either contraction or expansion of the heme core or the pyrrole rings. Asymmetric B_{1g} and B_{2g} distortions eliminate the C_mC_m and the N_pFeN_p symmetry axis, respectively, thus lowering the symmetry to C_{2v}. Antisymmetric A_{2g} distortions eliminate the symmetry of the pyrroles but maintain the 4-fold symmetry of the macrocycle, thus giving rise to C_{4h}.

In this paper we investigate two structural sensitive Raman modes of the oxygenated subunits, i.e., the oxidation marker line at 1375 cm^{-1} [ν_4 in the notation of Abe et al. (1978)] and the spin-marker line ν_{10}. As it has been shown for several heme proteins (Schweitzer-Stenner, 1989; Schweitzer-Stenner et al., 1989, 1991), the DPD of the ν_4 mode mainly responds to interactions between the heme core (i.e., N_p, C_α) and the ligands of the central iron because the corresponding Raman line gains major contributions from the $C_\alpha N_p$ stretching vibrations (Abe et al., 1978; Li et al., 1990). If the proximal imidazole eclipses the $N_p(I)$–Fe^{2+}–$N_p(III)$ line of the heme (Figure 2), the latter is affected by repulsive interactions between the pyrrole nitrogens $N_p(I)$ and $N_p(III)$ and the imidazole carbons C_δ and C_ϵ, respectively (Gellin & Karplus, 1977; Warshel, 1977; Shaanan, 1983; Friedman, 1985). As can be derived from the representations in Figure 1, this type of heme–protein coupling causes B_{1g} distortions of the heme (Schweitzer-Stenner, 1989), which increase with larger tilt angles Θ of the Fe^{2+}–N_ϵ[His(F8)] bond relative to the heme normal (Friedman, 1985). If the azimuthal angle ϕ between the $N_p(I)$–Fe^{2+}–$N_p(III)$ line and the projection of the proximal imidazole increases, the B_{1g} distortions of the N_p atoms are reduced, but asymmetric B_{1g}, B_{2g}, and A_{2g} distortions can now be induced by interactions between the imidazole carbons C_δ, C_ϵ, and the C_α of the pyrroles. Similar perturbations may also be induced by the sixth ligand of the iron atom. Fe^{2+}–O–O exhibits a bent conformation due to interactions with the distal part of the heme (Shaanan, 1983; Morikis et al., 1989). The relationship between symmetry-lowering distortions and the geometry of the Fe^{2+}–O_2 complex parallels that for the His(F8)–heme interaction.

Since the symmetry of the unperturbed ν_4 mode is A_{1g}, the corresponding c^{Γ}_{es} resulting from the distortions exhibit the symmetry $A_{1g} = A_{1g}(R) \times A_{1g}(j)$, $B_{1g} = A_{1g}(R) \times B_{1g}(j)$, $B_{2g} = A_{1g}(R) \times B_{2g}(j)$, and $A_{2g} = A_{1g}(R) \times A_{2g}(j)$.

The spin marker ν_{10} is constituted by C_mC_α and $C_\alpha C_\beta$ stretching vibrations. Its D_{4h} symmetry is B_{1g}, which is mainly perturbed by the PS at the pyrroles. This interaction is modulated by noncovalent contacts between the PS and aminio acid residues of the heme cavity (Wedekind et al., 1985; Schweitzer-Stenner et al., 1989; Bobinger et al. 1990). The PS of the heme group are displayed in Figure 2. By use of the diagrams in Figure 1 the following relationship between the distinct PS and symmetry-lowering distortions can be deduced. Assuming that identical PS should be regarded as sterically equivalent, the vinyls at $C_\beta(2)$ and $C_\beta(4)$ cause an antisymmetric A_{2g} distortion, whereas an asymmetric B_{2g} distortion is provided by the propionic acids at $C_\beta(6)$ and $C_\beta(7)$. B_{2g} and A_{2g} distortions are also induced by the methyls attached to $C_\beta(1)$, $C_\beta(3)$, $C_\beta(5)$, and $C_\beta(8)$. The matrix elements $c^\Gamma{}_{es}$ of the ν_{10} mode corresponding to these PS-induced distortions exhibit the symmetries $A_{2g} = B_{1g}(R) \times B_{2g}(j)$ and $B_{2g} = B_{1g}(R) \times A_{2g}(j)$. Asymmetric B_{1g} distortions are only provided if identical but sterically inequivalent PS cause different perturbations of the corresponding C_β atoms. In the intact HbA, this holds for the vinyls at $C_\beta(2)$ and $C_\beta(4)$ (Shaanan, 1983). For the ν_{10} mode the symmetry of the thus-induced $c^\Gamma{}_{es}$ is $A_{1g} = B_{1g}(R) \times B_{1g}(j)$.

Hence we can utilize the vibronic coupling matrix elements $c^\Gamma{}_{es}$ of the modes ν_4 and ν_{10} as suitable tools to elucidate the perturbations of the heme. They were derived from the experimentally observed DPDs by using them as free parameters in an expression of the polarizability tensor formulated in terms of a fifth-order time-dependent theory (TDR: time-dependent perturbation theory of Raman scattering) which has been described in detail elsewhere [cf. Schweitzer-Stenner (1989) and Schweitzer-Stenner et al. (1991)].

Computation of Raman Titration Curves. The vibronic coupling parameter $c^\Gamma{}_{es}$ described in eq 3 only considers one conformational type of heme groups to be present. In reality, due to conformational fluctuations between different substates and various protonation processes and conformational transitions in the apoprotein, many different conformational states of the molecule in equilibrium with each other and with different vibronic coupling parameters are present. In this case each conformation l exhibits distinct distortions $[\delta Q_j^{\Gamma(j)}]_l$ which can be related to a set of vibronic coupling parameters $(c^\Gamma{}_{es})_l$. Thus an effective polarizability tensor α^{eff} results from incoherent superposition of Raman scattering intensities from each specific conformation 1. This leads to the following equation for the corresponding effective vibronic coupling parameters (Schweitzer-Stenner, 1989):

$$c^\Gamma{}_{es} = \{\sum_l X_l (c^\Gamma{}_{es})_l^2\}^{1/2} \quad (4)$$

where X_l denotes the molar fraction of the lth conformation. The protonation of titrable groups in the protein can change the conformation, such that each protonation state of the molecule is related to a distinct conformational set of the heme group. In this case the X_l relate to the molar fractions of each titration state and $(c^\Gamma{}_{es})_l$ are effective vibronic coupling parameters owing to the subset of conformational states in each titration state.

Hence, by fitting eq 4 to the RTCs (Raman titration curves) [i.e., the representation of $c^\Gamma{}_{es}$(pH)], one derives the pK values of the involved amino acid residues and the vibronic coupling parameters $(c^\Gamma{}_{es})_l$ of each protonation state.

Materials and Methods

Preparation of Isolated Subunits. Human adult hemoglobin was prepared from freshly drawn blood by standard procedures (Brunner & Sussner, 1972). To obtain isolated subunits, we employed the protocol reported by Bucci et al. (1965). The pH value of the α^{SH}-oxyHbA and β^{SH}-oxyHbA solution was adjusted by dialyzing against 0.1 M Bis-Tris and Tris buffers. The concentration of the samples was 0.3 mM as derived from the optical absorbance measured with a Hewlett-Packard diode array spectrometer. At this concentration β^{SH}-oxyHbA is predominantly maintained in its tetrameric β_4-conformation independent of pH in the region between 6 and 9, whereas nearly 60% of α^{SH}-oxyHbA is in the monomeric and 30% in the dimeric α_2-state (McDonald et al., 1987).

Measurement of Polarized Raman Spectra. The exciting radiation was obtained from an argon ion laser (Spectra Physics) and an optically pumped dye laser using Rhodamine 110 (Spectra Physics) for the wavenumber region between 18 500 and 17 000 cm^{-1}. The experimental setup has been described in detail by el Naggar et al. (1985). The measured Raman spectra were measured and digitized on a microcomputer for further analysis. To calculate the correct height of the Raman lines, a computer program was employed to substract fluorescence background and to decompose complex spectra into distinct Lorentz lines of defined width and height (Stichternath, 1989). To obtain the resonance excitation profiles (REPs) polarized parallel $[E_\parallel(\Omega_L)]$ and perpendicular $[E_\perp(\Omega_L)]$ to the scattering plane, the relative intensities thus obtained were corrected for the frequency dependence, the transmission of the spectrometer, the power of the incident laser light, and absorption. The depolarization ratio (DPR) was calculated by

$$\rho(\Omega_L) = E_\parallel(\Omega_L)/E_\perp(\Omega_L) \quad (5)$$

Fitting Procedure. A program called MINUITL from the CERN library was used in a least-squares fit to the experimental DPDs and REPs. In a first approximation all fits were carried out in the framework of Gouterman's four-orbital model, which imposes the following restrictions on the vibronic coupling parameters (Schweitzer-Stenner et al., 1991):

$$c^{B_{1g}}{}_{QQ} = -c^{B_{1g}}{}_{BB} \qquad c^{B_{2g}}{}_{QQ} = -c^{B_{1g}}{}_{BB} \quad (6)$$

In most cases a satisfactory fit could not be obtained under these restrictions. Consequently, they have been relaxed and $c^\Gamma{}_{QQ}$ and $c^\Gamma{}_{BB}$ ($\Gamma = B_{1g}, B_{2g}$) were used as free parameters.

The quality of the fits was judged by means of the error value calculated by

$$f_{min} = \{\sum \chi_i^2/(N\sigma_i^2)\}^{1/2} \quad (7)$$

where χ_i^2 is the χ^2 value of the ith data point with respect to the best fit and σ_i is its statistical error. N denotes the number of data points.

In order to estimate the statistical errors of the vibronic coupling parameters, we calculated the normalized error value f/f_{min} as a function of the distinct parameters $c^\Gamma{}_{es}$ in the vicinity of the respective minimum of the χ^2 function. It turned out that inappropriate fits are obtained for f/f_{min} larger than 1.02. Thus we considered $\delta c^\Gamma{}_{es} = \pm|c^\Gamma{}_{es}(f_{min}) - c^\Gamma{}_{es}(1.02 f_{min})|$ as the statistical error of the vibronic coupling parameter $c^\Gamma{}_{es}$.

Since B_{1g}- and B_{2g}-type contributions to the polarizability tensor cannot be discriminated by polarization experiments on randomly oriented molecules, we omitted all $c^{B_{2g}}{}_{es}$ parameters in the fit to the data. Thus the vibronic coupling parameters $c^{B_{1g}}{}_{es}$ may also reflect some minor contributions from B_{2g}-type coupling to the scattering tensor. B_{1g}-type coupling, however, can be expected to be predominant for both lines investigated, because the ν_{10} mode exhibits B_{1g} symmetry in D_{4h} and the N_p atoms mainly involved in the heme–protein

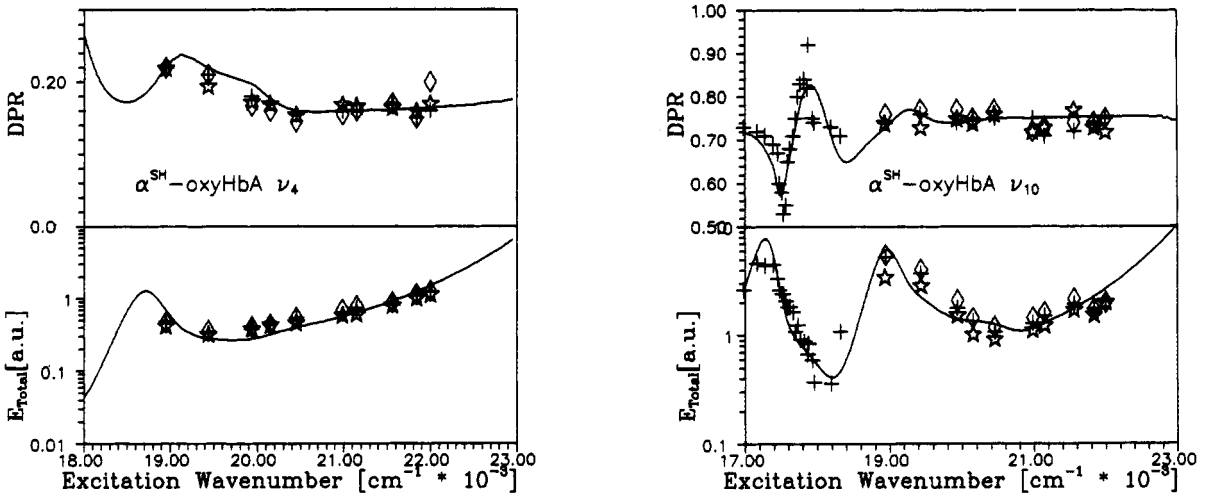

FIGURE 3: DPD and REPs of the ν_4 and ν_{10} mode in α^{SH}-oxyHbA. The data were measured at pH = 6.0 (☆), 7.1 (+), and 8.0 (◇). The solid lines result from the fit to the data.

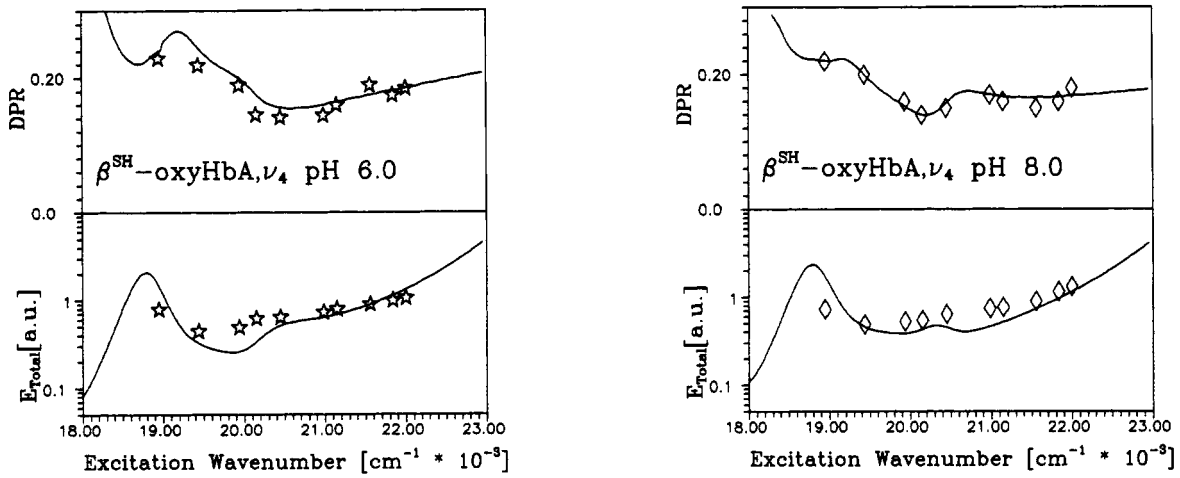

FIGURE 4: DPD and REPs of the ν_4 mode in β^{SH}-oxyHbA measured at pH = 6.0 and 8.0. The solid lines result from the fit to the data.

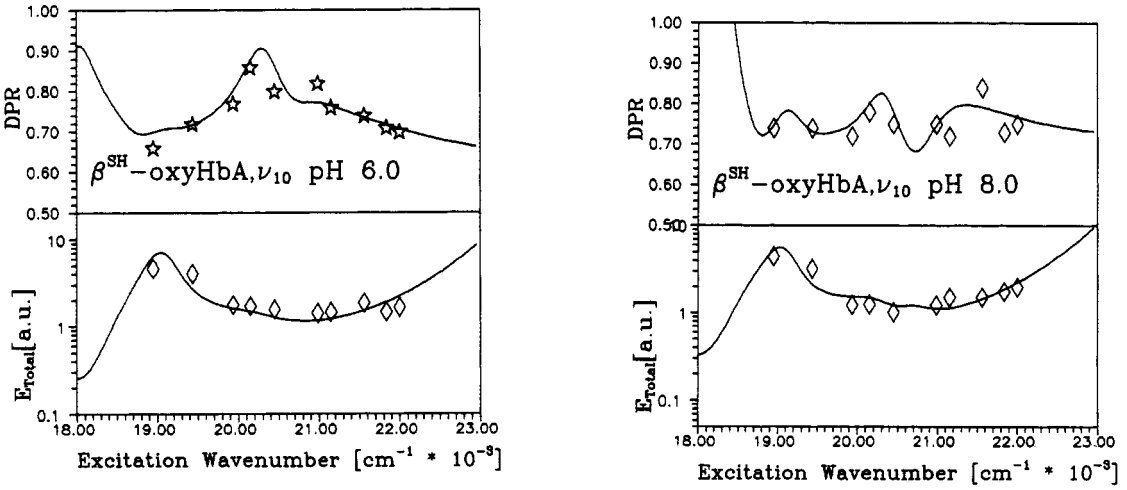

FIGURE 5: DPD and REPs of the ν_{10} mode in β^{SH}-oxyHbA measured at pH = 6.0 and 8.0. The solid lines result from the fit to the data.

interaction affecting the ν_4 mode cannot contribute to B_{2g}-type coupling (Figure 1).

To express the copuling parameters c^{Γ}_{es} in absolute units (cm^{-1}), we considered explicitly their contribution to the fifth-order term of the polarizability tensor as described in detail by Schweitzer-Stenner et al. (1991) and Bobinger et al. (1991). The remaining multimode contributions to the fifth-order term are represented by an effective helping phonon (Schweitzer-Stenner & Dreybrodt, 1985; Bobinger et al., 1989; Schweitzer-Stenner et al., 1991).

Results and Discussion

Comparison of α^{SH}-OxyHbA with β^{SH}-OxyHbA. We have measured the polarized REPs of the ν_4 and ν_{10} modes of both α^{SH}-oxyHbA and β^{SH}-oxyHbA, at various pHs between 6.0 and 8.5. From these data the corresponding DPDs and total REPs were derived. Representative data sets observed at pH = 6.0, 7.1, and 8.0 (α^{SH}-oxyHbA) and at pH = 6.0 and 8.0

Table I: Vibronic Coupling Parameters c^{Γ}_{es} Derived from the DPDs and REPs of the ν_4 and ν_{10} Modes Shown in Figures 1 and 2[a]

		β^{SH}-oxyHbA	
c^{Γ}_{es}	α^{SH}-oxyHbA	pH = 6.0	pH = 8.0
Vibronic Coupling Parameters of the ν_4 Mode			
$c^{A_{1g}}_{QQ}$	50 ± 7	102 ± 15	136 ± 20
$c^{A_{1g}}_{QB}$	99 ± 15	130 ± 20	138 ± 20
$c^{A_{1g}}_{BB}$	59 ± 4	53 ± 4	55 ± 4
$c^{B_{1g}}_{QQ}$	−15 ± 5	−45 ± 15	−144 ± 25
$c^{B_{1g}}_{QB}$	29 ± 5	20 ± 5	56 ± 10
$c^{B_{1g}}_{BB}$	22 ± 3	−27 ± 3	−21 ± 3
$c^{A_{2g}}_{QB}$	−36 ± 10	−58 ± 10	−73 ± 10
Vibronic Coupling Parameters of the ν_{10} Mode			
$c^{A_{1g}}_{QQ}$		60 ± 10	134 ± 20
$c^{A_{1g}}_{QB}$		30 ± 5	20 ± 5
$c^{A_{1g}}_{BB}$		5 ± 5	5 ± 5
$c^{B_{1g}}_{QQ}$	−41 ± 5	−10 ± 4	−20 ± 5
$c^{B_{1g}}_{QB}$	163 ± 10	179 ± 10	145 ± 8
$c^{B_{1g}}_{BB}$	41 ± 5	18 ± 3	26 ± 3
$c^{A_{2g}}_{QB}$		11 ± 5	54 ± 10

[a] All parameters are given in units of cm^{-1}.

(β^{SH}-oxyHbA) are displayed in Figures 3–5. The solid lines result from the fits to the data. The corresponding coupling parameters and their statistical errors are listed in Table I.

While the DPDs and REPs of both α^{SH}-oxyHbA modes are pH-independent, a significant pH dependence is obtained for β^{SH}-oxyHbA. This finding correlates with the observation that only the isolated β-subunits exhibit a Bohr effect (Kurtz & Bauer, 1978) (in the tetrameric and the monomeric form). It clearly shows that the heme in β^{SH}-oxyHbA is more sensitive to changes of the protein structure than in α^{SH}-oxyHbA. A detailed discussion of the pH-induced variations of β^{SH}-oxyHbA is given under pH Dependence of Vibronic Coupling Parameters.

The vibronic coupling paramters listed in Table I show that in both subunits B_{1g}- and A_{2g}-type coupling processes contribute to the scattering tensor of the ν_4 line. These are caused by distortions of the same symmetry. With the exception of the intrastate coupling parameters c^{Γ}_{BB} all c^{Γ}_{es} are significantly larger in β^{SH}-oxyHbA than in α^{SH}-oxyHbA.

As mentioned in the introduction, B_{1g} distortions acting on the ν_4 mode are mainly caused by repulsive interactions between the tilted ligands [i.e., C_δ, C_ϵ of His(F8), O_2] and pyrroles I and III (N_p, C_α). Thus they increase when the tilt angles Θ of the ligands become larger (Gellin & Karplus, 1977; Friedman et al., 1983, 1990; Friedman, 1985). Consequently, our data suggest that the O–O bond or the proximal imidazole are more tilted in β^{SH}-oxyHbA than in α^{SH}-oxyHbA. Crystallographic data on intact oxyHbA reported by Shaanan (1983), however, show that the proximal imidazole is more tilted in the β- than in the α-subunits, whereas the tilt angle of O–O is slightly larger in the β- than in the α-chains. This suggests that the proximal rather than the distal ligand is involved in the heme–protein interaction giving rise to the different B_{1g} distortions of the ν_4 mode in both subunits.

The antisymmetric contributions to the ν_4 mode (i.e., $c^{A_{2g}}_{QB}$) must be assigned to perturbations via the pyrrole carobns C_α and C_β, because C_m and N_p do not contribute to A_{2g}-type vibronic coupling (cf. the A_{2g} diagram in Figure 1). Hence our data suggest that the symmetry of the pyrrole rings is lowered by antisymmetric distortions. In β^{SH}-oxyHbA this asymmetry is more pronounced than in α^{SH}-oxyHbA (cf. the parameters $c^{A_{2g}}_{QB}$ in Table I) and is modulated by pH-induced heme–protein interaction.

Two possible explanations for the A_{2g} distortions of the ν_4 mode can be given. Since these distortions are caused by perturbations at the pyrroles, one may expect that they are due to asymmetric interactions between the pyrroles and their PS (model 1). The vinyls attached to $C_\beta(2)$ and $C_\beta(4)$ are appropriate candidates because their interactions with the macrocycle can induce A_{2g} distortions (cf. Figures 1 and 2). This type of interaction is known to decrease if the vinyls move out of the macrocycle plane (Hsu, 1970; Findsen et al., 1988). Thus the larger A_{2g} distortion found for β^{SH}-oxyHbA would suggest a more in-plane configuration of the vinyls.

A_{2g} distortions acting on the ν_4 mode, however, can also be assigned to interactions between the proximal imidazole and the C_α atoms of pyrroles I and III. In this case they are minimal, if the imidazole eclipses the $N_p(I)$–Fe^{2+}–$N_p(III)$ line, and maximal, if the imidazole eclipses one of the $C_\alpha(I)$–Fe^{2+}–$C_\alpha(III)$ lines. The latter situation corresponds to an azimuthal angle of nearly 20°. Since $c^{A_{2g}}_{QB}(\beta)$ is larger than $c^{A_{2g}}_{QB}(\alpha)$, this model predicts that the imidazole exhibits a larger azimuthal angle in β^{SH}- than in α^{SH}-oxyHbA.

It is instructive to compare the predictions of these two models with the X-ray data on intact oxyhemoglobin as reported by Shaanan (1983). We assume that the α- and β-subunits in the tetramer resemble the isolated subunits. While the vinyl side chain on pyrrole II is in plane in both subunits, it is significantly out of plane in pyrrole III. Moreover, with respect to the heme it is more tilted on pyrrole III in the β- than in the α-chain. This contradicts to the prediction of model 1. The azimuthal angle of the Fe^{2+}–N_ϵ[His(F9)] bond, however, is significantly larger in the β- than in the α-chains, in accordance with the prediction of model 2. As a consequence we assign the A_{2g} distortion of the ν_4 mode to interactions between the proximal imidazole and the C_α atoms of pyrroles I and III.

The crystallographic data argue against the possibility that the O–O bond contribute to the antisymmetric perturbation of the heme core. While in the α-subunit O–O is forced to eclipse the $N_p(I)$–Fe^{2+}–$N_p(III)$ line by steric interactions with the heme cavity, it is free to rotate over a large range about its equilibrium position. Thus its influence on the heme should be nearly isotropic. As a consequence, one suspects that the large difference in the A_{1g}-type coupling parameters of the ν_4 mode (i.e., $c^{A_{1g}}_{QQ}$, $c^{A_{1g}}_{QB}$) of the both chains is at least partially caused by interactions between O_2 and the heme. Further experiments are necessary to clarify this point.

The differences in the coupling properties of the ν_{10} mode in α^{SH}-oxyHbA and β^{SH}-oxyHbA are even more compelling than those of the ν_4 mode. In the resonant and preresonant region of the Q_v-band, the $\nu_{10}(\alpha)$ does not exhibit a dispersion of its DPR. In order to test whether this also holds for the region of the Q_0-band, we have measured the polarized REPs between 17 000 and 18 500 cm^{-1} by means of a dye laser pumped by the 514-nm line of the argon ion laser. As shown in Figure 3 the DPR exhibits a sharp minimum–maximum structure at 17 300 cm^{-1} similar to what has been obtained for this mode in oxyHbA and ferrocytochrome c (Schweitzer-Stenner & Dreybrodt, 1985; Bobinger et al., 1989). The theoretical analysis reveals that this DPD is nearly exclusively caused by multimode contributions from low-frequency modes different from ν_{10}. In the applied TDR theory they contribute to a term of the polarizability tensor formulated in fifth-order time-dependent perturbation theory (Schweitzer-Stenner, 1989; Schweitzer-Stenner et al., 1991; Bobinger et al., 1989, 1991). Thus, it is confirmed that neither $c^{A_{1g}}_{es}$ nor $c^{A_{2g}}_{es}$ coupling contributes to the Raman scattering at the $\nu_{10}(\alpha)$ mode. This

suggests that asymmetric B_{1g} and B_{2g} distortions are absent. Since it is difficult to discriminate between the contributions of $c^{B_{1g}}{}_{es}$ and $c^{B_{2g}}{}_{es}$, we cannot rule out that $c^{B_{2g}}{}_{es}$ coupling exists which would reflect antisymmetric A_{2g} distortions.

In contrast to the situation in α^{SH}-oxyHbA the ν_{10} mode in β^{SH}-oxyHbA exhibits a significant DPD depending on pH (Figure 4). The analysis reveals contributions from A_{1g} and A_{2g} coupling ($c^{A_{1g}}{}_{es}$ and $c^{A_{2g}}{}_{QB}$) which are related to asymmetric B_{1g} and B_{2g} distortions. Thus the DPDs of $\nu_{10}(\alpha)$ and $\nu_{10}(\beta)$ provide compelling evidence that the distortions caused by heme–protein coupling are drastically smaller in α^{SH}-oxyHbA compared to β^{SH}-oxyHbA. The vibronic coupling parameters of the ν_{10} mode predominantly reflect the interactions between the PS and the pyrroles. Therefore, to interpret its $c^{\Gamma}{}_{es}$, we apply the relationship between the PS of the pyrroles and the symmetry of the corresponding distortions which is outlined in the introductory section. There we have shown that antisymmetric B_{2g} distortions can be induced by the proprionic acids and also by the methyls. If, however, these groups are equivalent with regard to their interaction with the pyrroles, such distortions do not exist. Thus both methyl and propionic acid must be regarded as equivalent in α^{SH}-oxyHbA but not in β^{SH}-oxyHbA. Asymmetric B_{1g} distortions are interpreted to be indicative different interactions between C_β atoms and identical PS which exhibit different steric arrangements with respect to the heme. Its absence in α^{SH}-oxyHbA therefore indicates that all its identical PS are equivalent, whereas they are inequivalent in β^{SH}-oxyHbA.

A reasonable rationale for the different PS–heme interactions in the two types of isolated subunits can be given by utilizing the crystallographic data on the α- and β-hemes in the intact oxygenated molecule. The single-crystal data (Shannan, 1983) show that the porphyrin macrocycle is nearly planar; i.e., pyrrole rings I–IV form angles of 3°, 4°, 0°, and 1°, respectively. In the β-subunit the heme is in a more ruffled conformation, the angles between the pyrrole rings I–IV and the heme plane being −8°, 5°, 7°, and −7°. This is most probably due to the shorter contacts between Val(FG5)β and the vinyl on pyrrole III (Shaanan, 1983). Assuming that this holds approximately also for the isolated subunits, we suggest from our data that the capability of the PS to lower the symmetry of the macrocycle is larger in a ruffled that in a planar conformation. This is in accordance with novel Raman studies on ruffled nickel(II) octaethylporphyrin where the two ethyl groups of a tilted pyrrole group give rise to an asymmetric B_{2g} distortion due to their different orientations with respect to the pyrrole plane (Bobinger et al., 1991).

Correlation with Protein Dynamic Studies. Wintherhalter and DiIorio (1987) investigated the kinetics of CO rebinding to the isolated subunits at various temperatures between 40 and 300 K. From their data they derived distributions of the activation enthalpies (DAE) for ligand binding which result from different conformational substates with slightly different activation enthalpy barriers encountered by the last step of ligand binding (Austin et al., 1975; Frauenfelder et al., 1979, 1988; Parak et al., 1981). The authors found that α^{SH}-Hb exhibits a narrower DAE than β^{SH}-oxyHbA. This clearly suggests that the isolated β-chains are more heterogeneous than the α- chains. More recently, DiIorio et al. (1991) found that changes of the solvent's viscosity affect the DAE of β^{SH}-HbA rather than those of α^{SH}-HbA. This reveals that heme–protein coupling is significantly stronger in β^{SH}-HbA than in α^{SH}-HbA.

Our resonance Raman results parallel these findings. Moreover, they suggest that the conformational heterogenity, i.e., the number of conformational substates involved in the fluctuation of the heme, can be correlated with symmetry-lowering normal distortions of the porphyrin caused by imidazole–heme and PS–heme interactions. Since the Raman scattering process is much faster than the conversion between different substates (Parak & Knapp, 1985), the vibronic coupling paramters $c^{\Gamma}{}_{es}$ must be regarded as representing the time average of different static inhomogeneous distributions of the heme. They can therefore be written as

$$c^{\Gamma}{}_{es} = \{\sum_{\sigma} X_\sigma (c^{\Gamma}{}_{es})_\sigma^{2}\}^{1/2} \qquad (8)$$

where X_σ is the molar fraction of the hemes existing in the substate σ. The corresponding coupling parameters of this substate are denoted by $(c^{\Gamma}{}_{es})_\sigma$.

Hence the correlation between the DAE of the isolated HbA chains and the respective vibronic coupling parameters seems to indicate that the conformational substates differ in their symmetry and their vibronic and electronic properties. Thus increasing the number of substates involved in the conformational fluctuation increases the apparent asymmetric distortion of the heme. It can be further argued that ruffling of the porphyrin macrocycle in the β-chain increases the conformational disorder by coupling interactions between amino acid residues of the protein and the PS to the heme. Consequently, the more disordered heme of β^{SH}-oxyHbA is sensitive to perturbations of the protein, such as those caused by protonation of amino acid residues (Bohr effect) and changes of the protein–solvent interaction. Further studies of the heme distortions at low temperatures are required to explore in more detail the correlation between conformational substates and vibronic coupling parameters. They are underway in our laboratory.

pH Dependence of Vibronic Coupling Parameters. The Raman titration curves (RTCs; cf. the theoretical background section) of some representative vibronic coupling parameters of both β^{SH}-oxyHbA modes are shown in Figure 6. As shown under Materials and Methods, the $c^{\Gamma}{}_{es}$ must now be regarded as effective parameters and can be calculated by use of eq 4. We assume that each protonation state of the protein causes a significant distortion of the corresponding heme. Therefore, in eq 4 the X_l relate to the molar fractions of the titration state. To compute these molar fractions, we assume that the three titrable groups which influence the β-chain of the intact oxyHbA [R-state Bohr effect; cf. Schweitzer-Stenner et al. (1986)] also govern the RTCs of β^{SH}-oxyHbA. Their pK values are 7.8, 6.6, and 5.8. The molar fractions of the corresponding titration states $[i, j, k]$ were calculated using the formalism given by Schweitzer-Stenner et al. (1986) (i, j, k = 0, 1 label the occupation of the Bohr groups and are related to the pK values 7.8, 6.6, and 5.8 respectively). The coupling parameters $(c^{\Gamma}{}_{es})_l = c^{\Gamma}{}_{es}(i,j,k)$ of the titration states are used as free paramters in the fits to the RTCs. This yields the solid lines in Figure 5 which provide a sound reproduction of the RTCs. Thus evidence is provided that the RTCs of β^{SH}-oxyHbA are governed by the same titrable groups as the R-state Bohr effect in the tetrameric HbA.

In order to check whether the Bohr effect of β^{SH}-oxyHbA can also be related to the same pK values reflected by the RTC, we rationalized the log $P(O_2)$–pH diagram for O_2 binding in Figure 7 [data taken from Kurtz and Bauer (1978)] in terms of the equation (Antonini & Brunori, 1970):

$$\log P_{50} = \text{const} + \sum_{p} \log \{[[H^+] + K_p(\text{Hb})]/[[H^+] + K_p(\text{oxyHbA})]\} \qquad (9)$$

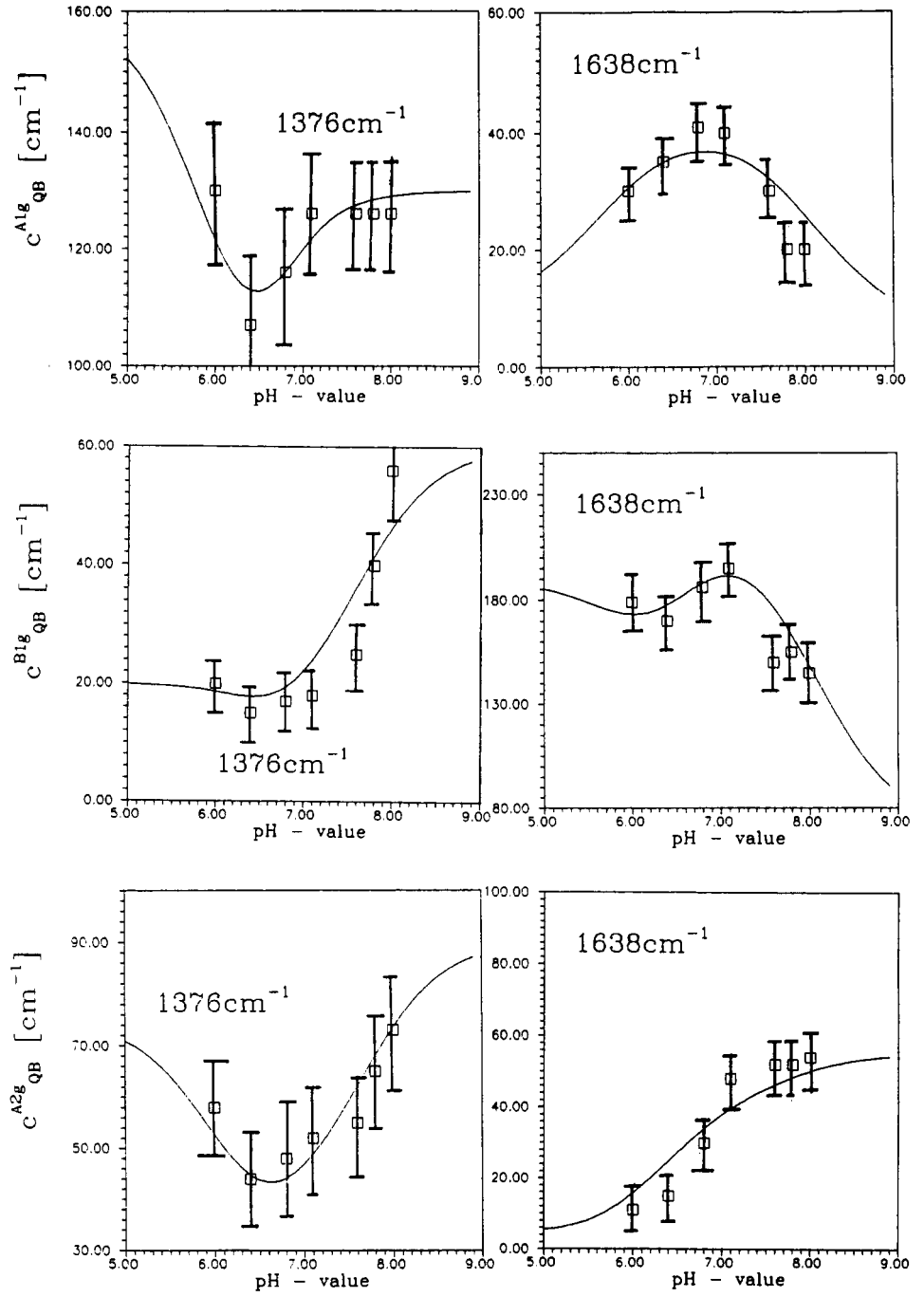

FIGURE 6: Three representative RTCs illustrating the pH dependence of the interstate vibronic coupling parameters $c^{A_1s}{}_{QB}$, $c^{b_1s}{}_{QB}$, and $c^{A_2s}{}_{QB}$ of the ν_4 and ν_{10} modes in β^{SH}-oxyHbA, respectively. The solid lines result from a fit to the data which was carried out by use of the titration model introduced in Schweitzer-Stenner et al. (1986).

where K_p(Hb) and K_p(oxyHbA) (p = 1, 2, 3) are the equilibrium constants for proton binding to the three titrable groups obtained in the unligated and oxygenated state, respectively. For the oxy state we used the pK values derived from the RTCs. The corresponding pKs of the deoxy state were obtained from the fit to the data which yields the solid line in Figure 7. It turns out that two different processes contribute to the Bohr effect. While pK_2 shifts from 7.1 to 6.6 upon ligation, pK_1 increases from 7.5 to 7.8 (inversed Bohr effect). The acid group 3 also shows a small inversed Bohr effect. It shifts from 5.6 in the deoxy state to 5.8 in the oxy state.

These results show that the Bohr effect of β^{SH}-oxyHbA can be explained in terms of the very same amino acid residues as the RTCs of the ν_4 and ν_{10} mode. Thus we establish a relationship between function and structure of the isolated subunits which correlates the pH dependence of ligand binding to β^{SH}-oxyHbA with the variation of the structural heterogenity of the prosthetic heme group.

In conclusion, this study provides evidence that the prosthetic heme group of β^{SH}-oxyHbA is significantly more distorted by asymmetric perturbations than that of α^{SH}-oxyHbA. By comparison with the protein dynamic studies of DiIorio et al. (1991) we find a correlation between heme distortion and the functional hetereogeneity of the two isolated subunits. This suggests that the apparent heme distortions depend on the number of conformational substates involved in the fluctuation of the molecule. Moreover, our data reveal that the heme–protein interactions affect the isolated β- rather than the α-chain. In β^{SH}-oxyHbA they give rise to pH-dependent vibronic coupling parameters, which can be rationalized in terms of the very same protonation processes as the corresponding Bohr effect.

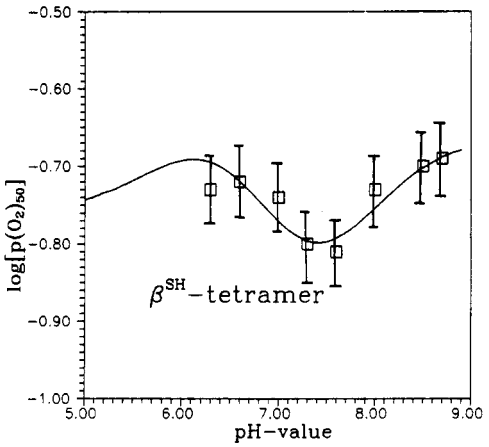

FIGURE 7: Plot of log P_{50} for oxygen binding to the tetrameric β^{SH}-Hb versus pH. The data and the error bars were taken from Kurtz and Bauer (1978). The solid line results from a fit to the experimental data by eq 4.

ACKNOWLEDGMENTS

We gratefully acknowledge that Prof. Beyersmann from the Chemistry Department helped us to isolate the subunits of human hemoglobin. Furthermore, we thank Diplom-Physiker Stefan Bradenbrink for reading the manuscript and Dr. Ernesto DiIorio for sending us a copy of his paper prior to publication.

Registry No. oxy-HbA, 9062-91-3; heme, 14875-96-8.

REFERENCES

Abe, M., Kitagawa, T., & Kyogoku, Y. (1978) *J. Chem. Phys. 69*, 4526–4534.

Antonini, E., & Brunori, M. (1971) *Hemoglobin and Myoglobin in their reactions with ligands*, Noth Holland Publishing Co., Amsterdam.

Austin, R. F., Beeson, K. W., Eisenstein, L., Frauenfelder, H., & Gusalus, I. C. (1975) *Biochemistry 14*, 5355–5373.

Baldwin, J. L., & Chotia, C. (1979) *J. Mol. Biol. 129*, 175–200.

Benesh, R. E., Ranney, M. H., Benesch, R., & Smith, G. M. (1961) *J. Biol. Chem. 236*, 2926–2929.

Bobinger, U., Schweitzer-Stenner, R., & Dreybrodt, W. (1989) *J. Raman Spectrosc. 20*, 191–202.

Bobinger, U., Stichternath, A., Dreybrodt, W., & Schweitzer-Stenner, R. (199) in *Proceedings of the XIIth International Conference on Raman Spectroscopy* (During, R., & Sullivan, J. F., Eds.) Wiley & Sons, New York, pp 530–531.

Bobinger, U., Schweitzer-Stenner, R., & Dreybrodt, W. (1991) *J. Phys. Chem. 95*, 7625–7635.

Brunner, H., & Sussner, A. (1973) *Biochim. Biophys. Acta 310*, 20–31.

Bucci, E., Fronticelli, C., Chiancone, E., Wyman, J., Antonini, E., & Rossi-Fanelli, A. (1965) *J. Biol. Chem. 12*, 183–192.

Collins, D. W., Fitchen, D. B., & Lewis, A. (1973) *J. Chem. Phys. 59*, 5714–5719.

DiIorio, E. E., Hiltpold, U. R., Filipovic, D., Winterhalter, K. H., Gratton, E., Vitrano, E., Cupane, A., Leone, M., & Cordone, M. (1991) *Biophys. J. 59*, 742–754.

El Naggar, S., Dreybrodt, W., & Schweitzer-Stenner, R. (1985) *Eur. Biophys. J. 12*, 43–49.

Findsen, L. A., Bocia, D. F., & Birge, R. R. (1988) *J. Chem. Phys. 88*, 7588–7598.

Frauenfelder, H., Petsko, G. A., & Tsernoglou, D. (1979) *Nature (London) 280*, 558–563.

Frauenfelder, H., Parak, F., & Young R. D. (1988) *Annu. Rev. Biophys. Biophys. Chem. 17*, 451–479.

Friedman, J. M. (1985) *Science 228*, 1274–1280.

Friedman, J. M., Scott, T. W., Stepnowski, R. A., Ikedo-Saito, M., & Yonetari, T. (1983) *J. Biol. Chem. 10*, 10564–10572.

Friedman, J. M., Campbell, B. F., & Noble, R. W. (1990) *Biophys. Chem. 37*, 43–59.

Gellin, B. R., & Karplus, M. (1977) *Proc. Natl. Acad. Sci. U.S.A. 74*, 801–805.

Gouterman, M. (1959) *J. Chem. Phys. 30*, 1139–1161.

Hsu, M. C. (1970) Ph.D. Thesis, University of Illinois, Urbana, IL.

Kurtz, A., & Bauer, C. (1978) *Biochem. Biophys. Res. Commun. 84*, 852–857.

Li, X.-Y., Czernuszewicz, R. S., Kincaid, J. R., Stein, P., & Spiro, T. G. (1990) *J. Phys. Chem. 94*, 47–61.

McClain, W. M. (1971) *J. Chem. Phys. 55*, 2789–2796.

McDonald, M. J., & Noble, R. W. (1972) *J. Biol. Chem. 247*, 4282–4287.

McDonald, M. J., Turci, S. M., Mrabet, N. T., Himelstein, B. P., & Bunn, H. F. (1987) *J. Biol. Chem. 262*, 5951–5956.

Morikis, D., Champion, P. M., Springer, B. A., & Sligar, S. G. (1989) *Biochemistry 28*, 4791–4799.

Parak, F., & Knapp, E. W. (1985) *Proc. Natl. Acad. Sci. U.S.A. 81*, 7088–7092.

Parak, F., Frolow, E. N., Mössbauer, R. L., & Goldanskii, V. I. (1981) *J. Mol. Biol. 145*, 825–833.

Schweitzer, R., Dreybrodt, W., Mayer, A., & El Naggar, S. (1982) *J. Raman Spectrosc. 13*, 139–147.

Schweitzer-Stenner, R. (1989) *Q. Rev. Biophys. 22*, 381–479.

Schweitzer-Stenner, R., & Dreybrodt, W. (1985) *J. Raman Spectrosc. 16*, 111–123.

Schweitzer-Stenner, R., Wedekind, D., & Dreybrodt, W. (1986) *Biophys. J. 49*, 1077–1088.

Schweitzer-Stenner, R., Wedekind, D., & Dreybrodt, W. (1989) *Biophys. J. 55*, 703–712.

Schweitzer-Stenner, R., Bobinger, U., & Dreybrodt, W. (1991) *J. Raman Spectrosc. 22*, 65–78.

Shaanan, B. (1983) *J. Mol. Biol. 171*, 31–59.

Shelnutt, J. A. (1980) *J. Chem. Phys. 72*, 3948–3958.

Shelnutt, J. A., & Oritz, V. (1985) *J. Phys. Chem. 89*, 4733–4739.

Spiro, T. G., & Strekas, T. C. (1974) *J. Am. Chem. Soc. 96*, 338–345.

Šrajer, V., & Champion, P. M. (1991) *Biochemistry 30*, 7390–7402.

Šrajer, V., Schomaker, K. T., & Champion, P. M. (1986) *Phys. Rev. Lett. 57*, 1267–1270.

Šrajer, V., Reinisch, L., & Champion, P. M. (1988) *J. Am. Chem. Soc. 110*, 6656–6670.

Stichternath, A. (1989) Diploma Thesis, University of Bremen.

Warshel, A. (1977) *Proc. Natl. Acad. Sci. U.S.A. 74*, 1789–1793.

Wedekind, D., Schweitzer-Stenner, R., & Dreybrodt, W. (1985) *Biochim. Biophys. Acta 830*, 224–232.

Winterhalter, K. H., & Colosimo, A. (1971) *Biochemistry 10*, 621–624.

Winterhalter, K. H., & Di Iorio, E. E. (1987) *Acta Haematol. 78*, 90–94.

Zgierski, M. Z., & Pawlikowski, M. (1982) *Chem. Phys. 65*, 335–367.